Research Article
CODEN (USA): IJPLCP

[Gade & Mahmood, 3(7): July, 2012]
ISSN: 0976-7126

INTERNATIONAL JOURNAL OF PHARMACY & LIFE SCIENCES

3D-QSAR studies on a diverse set of heterocyclic MMP inhibitors

Swetha Gade* and Shaik Mahmood[1]

*Bioinformatics Division, Department of Botany, Osmania University, Hyderabad, (A.P.) - India
1, Bioinformatics Division, Environmental Microbiology Lab., Department of botany, Osmania University, Hyderabad, (A.P.) - India

Abstract

We have performed three dimensional quantitative structure activity relationship (3D-QSAR) studies on a set of pyridinone derivatives acting as MMP inhibitors. We have carried out the Study using Comparative Molecular Field Analysis (CoMFA) and Comparative Molecular Similarity Indices Analysis (CoMSIA) approaches. Ligand molecular superimposition on the template structure was performed by the database alignment method. We have validated the training set of 47 molecules with a test set of 14 molecules for the improved predictivity of the model. CoMFA model yielded the best predictive values q^2_{cv}, 0.876; r^2 (non-cross-validated square of correlation coefficient), 0.968; F value, 244.63; r^2_{bs}, 0.977 with five components, and standard error of estimate (SEE), 0.055. The CoMSIA model yielded q^2_{cv}, 0.829; r^2, 0.983; F value, 383.035; r^2_{bs}, 0.986 with six components and SEE of 0.0041. We have analyzed the contour maps obtained from the study to reveal several key features responsible for the activity trends of inhibitors. The present study will further guide the design of novel, potent and selective MMP inhibitors.

Key-Words: Matrix metalloproteinase MMP-1 inhibitors, 3D-QSAR, CoMFA, CoMSIA

Introduction

Matrix metalloproteinases (MMP's) are a family of zinc dependent endoproteinases. MMP's form an integral part of cell's extra cellular matrix (ECM). Collectively, MMP's are capable of degrading complete ECM (1). Initially they were found in the metamorphosing organs of the anuran tadpole matrix, now they are known to be the major mediators of the ECM (2, 3). Undesirable changes in cell's ECM are the key reason for many diseases. cancer, arthritis and cardiovascular disorders are usually linked to the changes in the cell's (ECM) (4). These enzymes also play a vital role in many other important processes like cell proliferation, differentiation, migration, death, and cell–cell interactions (5). Recent studies have revealed that MMP's also have non matrix substrates such as chemokines, growth factors, and receptors, indicating the influence of MMPs on wider array of physiological and pathological processes (6).

*** Corresponding Author**
E.mail:swethareddy001@gmail.com,
moodbio@yahoo.com
Mob. +91-9290449000, +91-9849602498

MMPs belong to the metzincin family of enzymes that incorporate zinc ion in their active sites. The MMP family of enzymes consists of 28 members with many different physiological and pathological implications. These are released in the inactive form and are activated by a number of factors. Their function is to degrade different substrates of the ECM for tissue remodeling. Usually MMP's are regulated by tissue inhibitors of MMP (TIMP), these form a small endogenous inhibitor family of four enzymes. Imbalance in the levels of MMP and TIMP is held responsible in the development of pathological conditions (7, 8). Inflammatory conditions are almost always characterized by deregulated, often increased MMP activities (9).Enhanced activity of MMP-2 and MMP-9 which are also known as gelatinases is responsible for myocardial infarction, aneurysms, and atherosclerotic plaques. Increased activities of MMPs have been the major cause of unwanted tissue remodeling in the cardiovascular system, which increases the need for specific MMP inhibitors.(10-12) Currently, there is only one medically approved MMP inhibitor, which is a tetracycline derivative used in the treatment of periodontal disease. Studies are going on hydroxamate based inhibitors which are showing good in vitro inhibitory activities(13) but have a few limitations like low oral availability, poor in vivo stability, pharmacokinetic problems,(14, 15) and

undesirable side effects. Discovery of new inhibitors with better properties and less side effects is beneficial for therauptic use (16-18). In the present study, 3D-QSAR CoMFA and CoMSIA analyses are done on a series of potent MMP inhibitors (19) with the aim to identify key features responsible for inhibitory activity. Generated 3D-computational models can be used to explore useful suggestions for designing of new MMP inhibitors with improved potency.

Material and Methods

Molecular modeling

The three-dimensional structures of all molecules were constructed by using SYBYL programming package version 6.7 (20) on a Silicon Graphics Fuel workstation.

Energy minimization was performed using Tripos force field (21) and the Gasteiger-Huckel (22) charge with a distance-dependant dielectric and Powell conjugate gradient algorithm with convergence Criterion of 0.05kcal/mol. Further geometric optimization of these compounds was done using the semi-empirical program MOPAC 6.0 and applying the AM1 Hamiltonian (23). The MOPAC charges were used for entire calculations.

Data set

The in vitro biological activity data reported as IC_{50}, for inhibition of MMP-1 were taken from the published work by Ryuji Hayashi et al(19) and used for the current study (Table 1).

The reported IC_{50} values were converted into the corresponding pIC_{50} using the following formula:

$pIC50 = -\log IC50*10^{-6}$

Alignment

In the present study the MOPAC geometry optimized structures were aligned on the most active molecule among the given set. All the molecules were aligned by the 'Align Database' command available in SYBYL using maximum substructure. It adjusts the geometry of the molecules such that its steric and electrostatic fields match the fields of the template molecule. The aligned molecules are shown in Fig. 1.

CoMFA studies

The steric and electrostatic CoMFA potential fields were calculated at each lattice intersection of a regularly spaced grid of 2.0 A°. The grid box dimensions were determined automatically in such a way that region boundaries were extended beyond 4 A° in each direction from co-ordinates of each molecule. The Vander Waals potentials and Columbic terms, which represent steric and electrostatic fields, respectively, were calculated using Tripos force field. A sp^3 hybridized carbon atom with +1 charge served as probe atom to calculate steric and electrostatic fields.

CoMSIA studies

The CoMSIA (24) technique was introduced by Klebe in1994 in which similarity indices are calculated at different points in a regularly spaced grid for pre-aligned molecules. It has several advantages over CoMFA technique like greater robustness regarding both region shifts and small shifts within the alignments; no application of arbitrary cutoffs and more intuitively interpretable contour maps. In CoMSIA, a distance-dependent Gaussian-type physicochemical property has been adopted to avoid singularities at the atomic positions and dramatic changes of potential energy for those grids in the proximity of the surface. The standard settings (Probe with charge +1, radius $1A^0$ and hydrophobicity +1, hydrogen-bond donating +1, hydrogen-bond accepting +1, attenuation factor R of 0.3 and grid spacing 2 A^0) were used in CoMSIA to calculate five different fields viz. steric, electrostatic, hydrophobic, acceptor and donor.

Partial least square (PLS) analysis

To quantify the relationship between the structural parameters (CoMFA and CoMSIA interaction energies) and the biological activities, the PLS algorithm was used. The CoMFA descriptors were used as independent variables, and pIC_{50} values as dependant variables in partial least square regression analysis. Cross-validation partial least square method of leave-one-out (LOO) was performed to obtain the optimal number of components used in the subsequent analysis. The minimum sigma (column filtering) was set to 2.0 kcal/mol to improve the signal- to-noise ratio. The optimum number of principle components in the final non-cross-validated QSAR equations was determined to be that leading to the highest correlation coefficient (r^2) and the lowest standard error in the LOO cross validated predictions. The non-cross-validation was used in the analysis of CoMFA result and the prediction of the model. The same method was used for CoMSIA too, thereafter a full PLS was run using column filtering of 1.0 kcal/mol. Auto scaling was applied to all CoMSIA analysis.

Results and Discussion

The 3D-QSAR CoMFA and CoMSIA techniques were used for analyzing pyridinone derivatives acting as MMP-1 inhibitors. The leave-one-out partial least-squares (PLS) analysis of the obtained model yielded high cross-validated q^2-value of 0.876 (five components) and non-cross-validated correlation coefficient r^2 of 0.968. Table 1 lists structures, experimental activities, predicted activities and residual values of the training set and test set molecules by CoMFA and CoMSIA models. The statistical

parameters for the developed CoMFA and CoMSIA models are presented in Table 2. These correlation coefficients suggest that our model is reliable and accurate. Fig. 2 and 3 show correlation between the experimental and predicted activity values of molecules derived from CoMFA and CoMSIA respectively.

3D-QSAR contour analysis

The results obtained from CoMFA and CoMSIA were graphically interpreted through the Std.dev. Coefficient contour maps (Figures 4, 5). These contour maps provide a detailed understanding of the key structural features required for the activity of pyridinone derivatives and related compounds.

CoMFA contours:

The CoMFA contour maps have permitted an understanding of the steric and electrostatic requirements that represent the QSAR result. Fig. 4 (a-d) shows the contour maps derived from the CoMFA PLS model. The maps of most active compound 21 (Fig. 4a and b) and lowest active compound 52 (Fig. 4 c and d), were analyzed. The contour plots help to identify important regions where any change may affect the activity of molecule. Furthermore, they may be helpful in identifying important features contributing to increased activity of molecules. The steric interactions are represented by green and yellow colored contours whereas electrostatic interactions are displayed as red and blue contours.

The CoMFA steric map encompasses yellow contours corresponding to the regions in space where the steric bulk envisages the decrease in activity and the yellow polyhedron bordering 2, 4, 6 fluoro benzyl rings suggest that the steric substitutions at these rings are not favorable. Detrimental effect on the inhibitory potency is observed in molecules where this ring is replaced with groups like benzyl and isopropyl. Conversely, the green contour below the nitrogen of pyridinone ring reveals that, an increase in activity is anticipated due to increased steric bulk.

CoMFA electrostatic map of highest active molecule, displays one large red contour embedding the oxygen of pyridinone ring and another small red contour at the vicinity of F of benzyl ring where the partial negative charge is associated with increased activity. Large blue contour running from central joining Oxygen molecule to benzyl ring indicates area within the lattice where the electropositive properties of molecules describe an increase in activity.

CoMSIA contours

In addition to the steric and electrostatic fields, CoMSIA also defines the lipophilic, hydrogen bond donor, and acceptor fields that are generally not accessible with standard CoMFA 5(a-e).

CoMSIA steric contour map highlights the region around fluoro benzene ring where as in CoMFA steric map; we have seen the impact of groups near the pyridinone ring. CoMSIA electrostatic map gives almost same information as in CoMFA contour map except for a few more red contours around the flouro benzene ring. As shown in Figure 5(c), a hydrophilic area (white) appears near the oxygen of pyridinone ring. This clearly explains the reason for the increased activity of molecules 1-39 over other molecules. Molecules 40-67 do not incorporate nitrogen in the ring which is hydrophilic than sulfur. a hydrophobic region (yellow) is seen at the vicinity of R1 position of fluoro benzene ring. This indicates that any hydrophilic substitutions at this position will lead to decreased activity. Molecules having hydrophilic fluorine (53-57) at this position are showing comparatively lesser activity than the molecules that have hydrophobic groups (1-7). In the hydrogen bond acceptor field (Fig.5d), a large magenta polyhedron indicates that acceptor groups at that position increase activity. Molecules 1-39 which have oxygen in the vicinity of the contour have an advantage over other molecules. This is one of the reasons for the higher activity of the above. In the hydrogen bond donor field, (Fig.5e), the purple area denotes a region where a donor group is not favorable for the activity.

In this study, we have investigated the CoMFA and CoMSIA models on a set of 67 structurally diverse MMP inhibitors. These models demonstrated excellent internal and external predictive ability, which was shown by several strategies including cross validation.

Overall, the CoMFA model gave good results while the CoMSIA model was more valuable for the three fields that contributed significantly (hydrophobic, hydrogen bond acceptor, and hydrogen bond donor). The CoMSIA analysis indicated that variations in the activity are dominated by hydrophobic interactions. Additionally, the CoMSIA model suggests that a hydrogen bond acceptor may have a positive effect on the potency. The excellent correlation with several experimental studies suggests that these 3D-QSAR models are reliable, helping us to understand the binding interaction of these inhibitors and providing a helpful guideline for further lead optimization. The features derived from the above models bear a close correlation with the structural variations inherent in the training set, so other structurally distinct data may likely result in diverse features causing different conclusions. In summary, our preliminary findings may aid in identifying potent and specific compounds that

may be used as MMP inhibitors and offer more significant insights into the overall pharmacology of this system.

References

1. Page-McCaw A, Ewald AJ, & Werb Z (2007) Matrix metalloproteinases and the regulation of tissue remodelling. *Nat Rev Mol Cell Biol* 8(3):221-233.
2. Gross J & Lapiere CM (1962) Collagenolytic activity in amphibian tissues: a tissue culture assay. (Translated from eng) *Proc Natl Acad Sci U S A* 48:1014-1022 (in eng).
3. Gross J & Nagai Y (1965) Specific degradation of the collagen molecule by tadpole collagenolytic enzyme. (Translated from eng) *Proc Natl Acad Sci U S A* 54(4):1197-1204 (in eng).
4. Brinckerhoff CE & Matrisian LM (2002) Matrix metalloproteinases: a tail of a frog that became a prince. *Nat Rev Mol Cell Biol* 3(3):207-214.
5. Elkington PT, O'Kane CM, & Friedland JS (2005) The paradox of matrix metalloproteinases in infectious disease. (Translated from eng) *Clin Exp Immunol* 142(1):12-20 (in eng).
6. McCawley LJ & Matrisian LM (2001) Matrix metalloproteinases: they're not just for matrix anymore! (Translated from eng) *Curr Opin Cell Biol* 13(5):534-540 (in eng).
7. Brew K & Nagase H (2010) The tissue inhibitors of metalloproteinases (TIMPs): an ancient family with structural and functional diversity. (Translated from eng) *Biochim Biophys Acta* 1803(1):55-71 (in eng).
8. Spinale FG (2007) Myocardial matrix remodeling and the matrix metalloproteinases: influence on cardiac form and function. (Translated from eng) *Physiol Rev* 87(4):1285-1342 (in eng).
9. Parks WC, Wilson CL, & Lopez-Boado YS (2004) Matrix metalloproteinases as modulators of inflammation and innate immunity. (Translated from eng) *Nat Rev Immunol* 4(8):617-629 (in eng).
10. Spinale FG (2002) Matrix metalloproteinases: regulation and dysregulation in the failing heart. (Translated from eng) *Circ Res* 90(5):520-530 (in eng).
11. Creemers EE, Cleutjens JP, Smits JF, & Daemen MJ (2001) Matrix metalloproteinase inhibition after myocardial infarction: a new approach to prevent heart failure? (Translated from eng) *Circ Res* 89(3):201-210 (in eng).
12. Spinale FG, Coker ML, Bond BR, & Zellner JL (2000) Myocardial matrix degradation and metalloproteinase activation in the failing heart: a potential therapeutic target. (Translated from eng) *Cardiovasc Res* 46(2):225-238 (in eng).
13. Babine RE & Bender SL (1997) Molecular Recognition of Proteinminus signLigand Complexes: Applications to Drug Design. (Translated from Eng) *Chem Rev* 97(5):1359-1472 (in Eng).
14. Brown PD (1999) Clinical studies with matrix metalloproteinase inhibitors. (Translated from eng) *APMIS* 107(1):174-180 (in eng).
15. Coussens LM, Fingleton B, & Matrisian LM (2002) Matrix metalloproteinase inhibitors and cancer: trials and tribulations. (Translated from eng) *Science* 295(5564):2387-2392 (in eng).
16. Bramhall SR*, et al.* (2002) Marimastat as maintenance therapy for patients with advanced gastric cancer: a randomised trial. (Translated from eng) *Br J Cancer* 86(12):1864-1870 (in eng).
17. Bramhall SR, Rosemurgy A, Brown PD, Bowry C, & Buckels JA (2001) Marimastat as first-line therapy for patients with unresectable pancreatic cancer: a randomized trial. (Translated from eng) *J Clin Oncol* 19(15):3447-3455 (in eng).
18. Groves MD*, et al.* (2002) Phase II trial of temozolomide plus the matrix metalloproteinase inhibitor, marimastat, in recurrent and progressive glioblastoma multiforme. (Translated from eng) *J Clin Oncol* 20(5):1383-1388 (in eng).
19. Hayashi R, Jin X, & Cook GR (2007) Synthesis and evaluation of novel heterocyclic MMP inhibitors. (Translated from eng) *Bioorg Med Chem Lett* 17(24):6864-6870 (in eng).
20. Tripos (2000) SYBYLSt. Louis, MO), 6.7.
21. Clark M, Cramer RD, & Van Opdenbosch N (1989) Validation of the general purpose tripos 5.2 force field. *Journal of Computational Chemistry* 10(8):982-1012.
22. Gasteiger J & Marsili M (1980) Iterative partial equalization of orbital electronegativity—a rapid access to atomic charges. *Tetrahedron* 36(22):3219-3228.
23. Stewart JJ (1990) MOPAC: a semiempirical molecular orbital program. (Translated from eng) *J Comput Aided Mol Des* 4(1):1-105 (in eng).
24. Klebe G, Abraham U, & Mietzner T (1994) Molecular similarity indices in a comparative analysis (CoMSIA) of drug molecules to correlate and predict their biological activity. (Translated from eng) *J Med Chem* 37(24):4130-4146 (in eng).

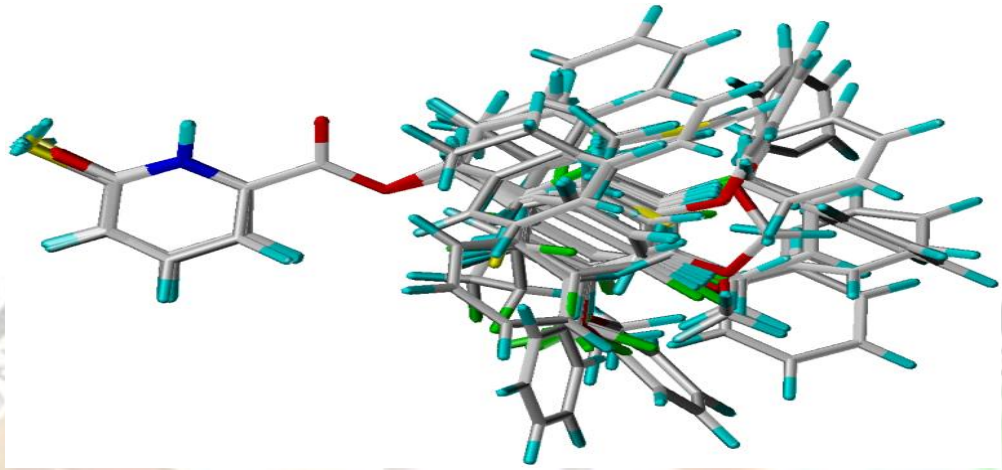

Fig. 1: Alignment of all molecules used for molecular field generation

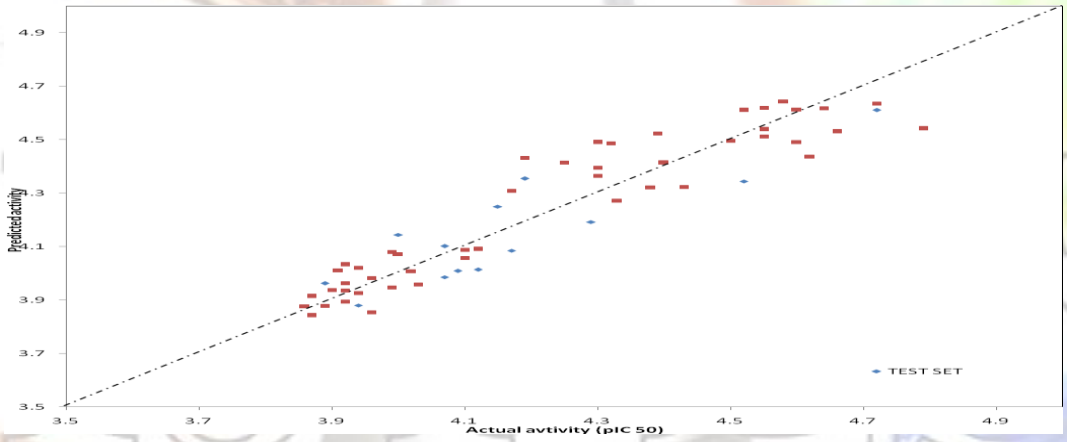

Fig. 2: Graph of Predicted versus actual activity from CoMFA analysis

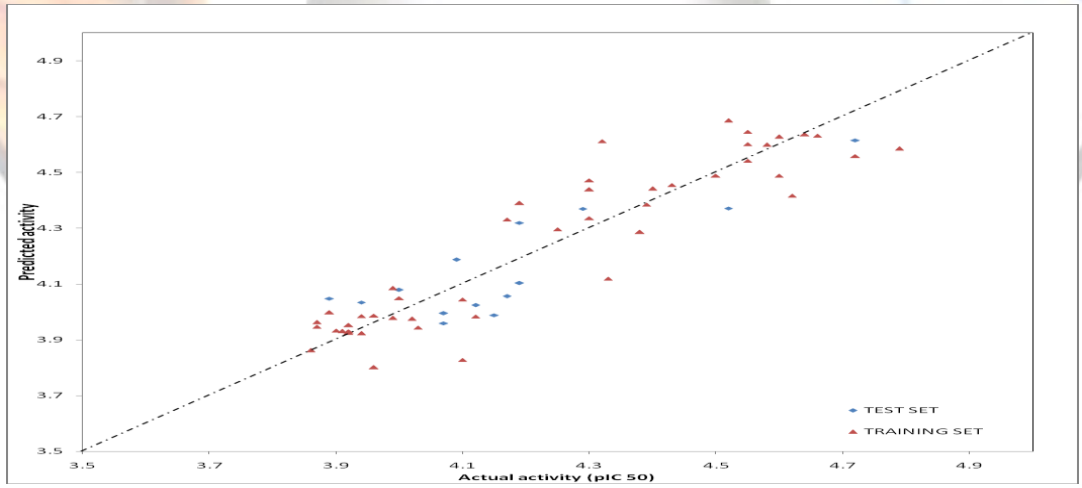

Fig. 3: Graph of Predicted versus actual activity from CoMSIA analysis

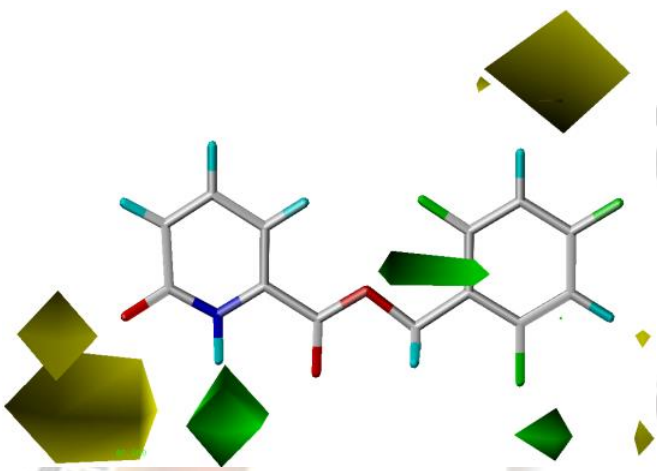

4A

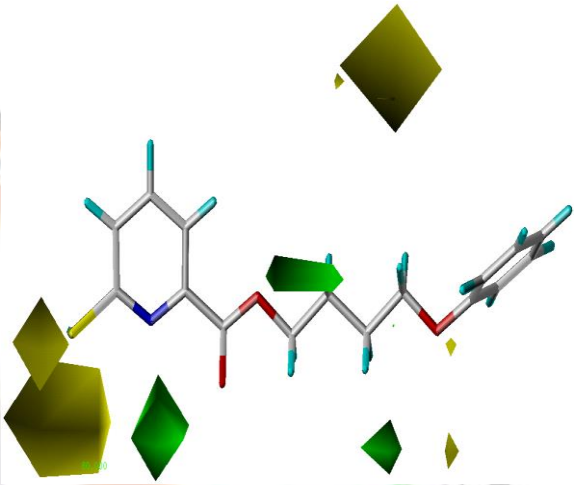

4B

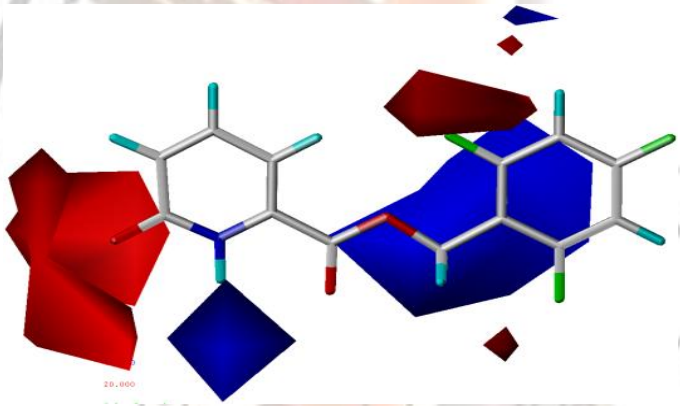

4C

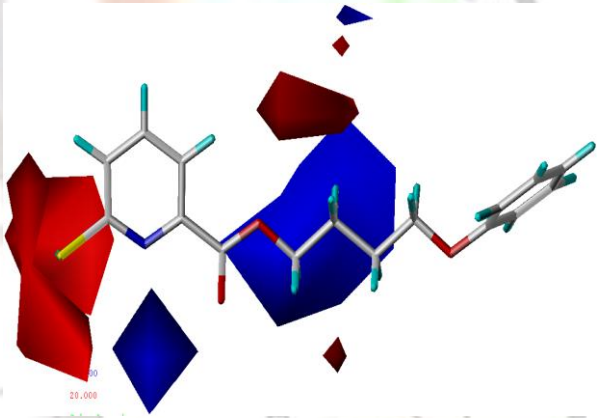

4D

Fig. 4: Comfa contour maps: A: CoMFA steric contour map of most active MMP-1 inhibitor (21). B: CoMFA steric contour map of least active MMP-1 inhibitor (52). Regions of favorable steric interactions are shown in green; sterically unfavorable regions are shown in yellow. C: CoMFA electrostatic contour map of most active MMP-1 inhibitor (21). D: CoMFA electrostatic contour map of least active MMP-1inhibitor (52) Positive potential areas in blue where more positively charged groups increase activity; Negative potential favored areas in red where more negatively charged groups increase activity.

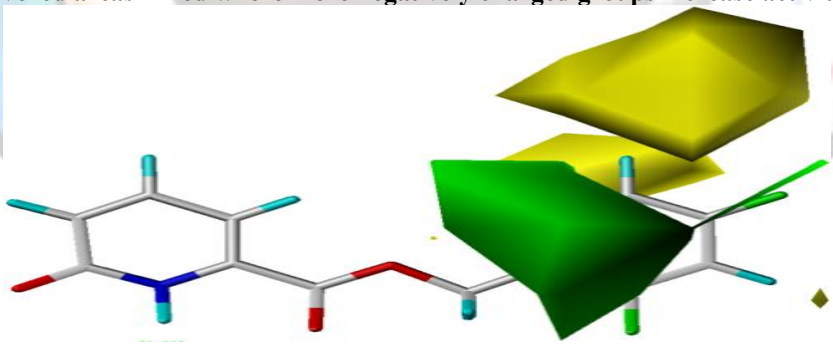

5A

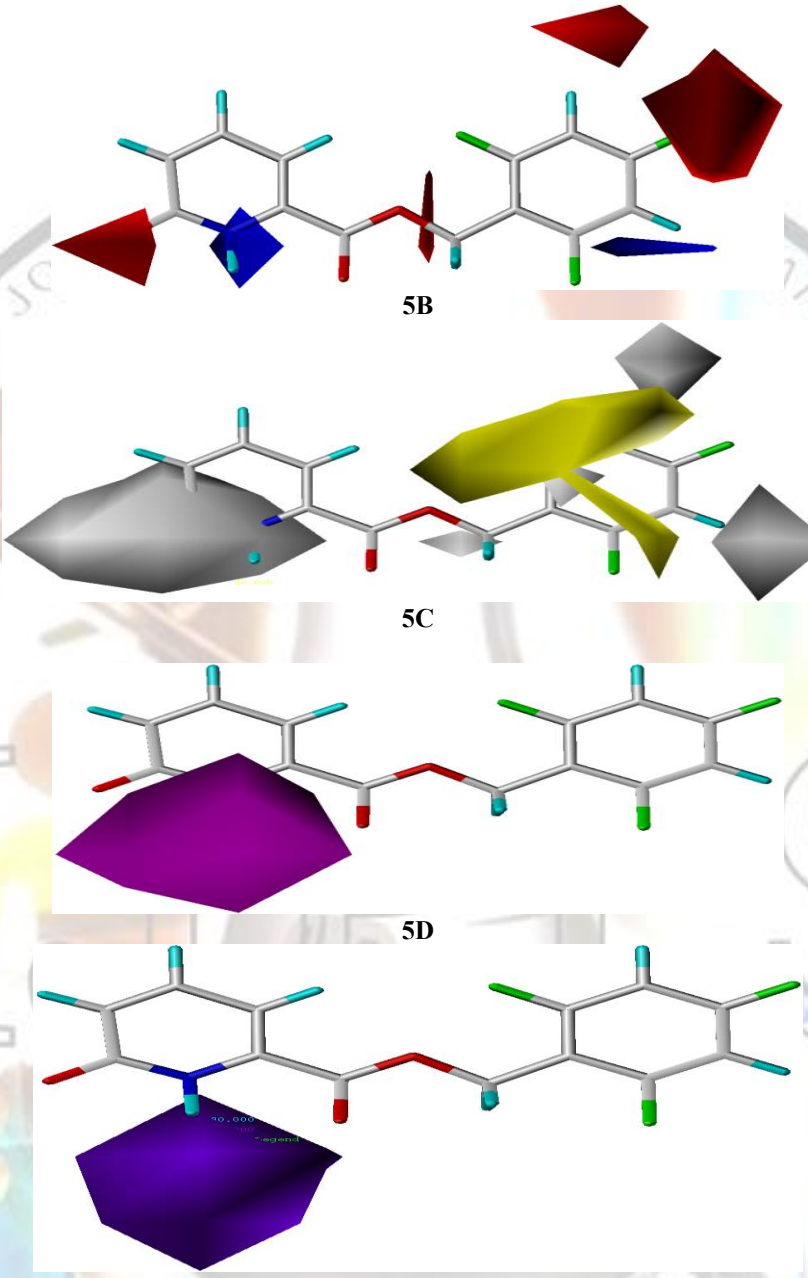

5B

5C

5D

5E

Fig. 5: Comsia contour maps: A. CoMSIA steric contour map of most active MMP-1 inhibitor. Regions of favorable steric interactions are shown in green; sterically unfavorable regions are shown in yellow activity. B. CoMSIA electrostatic contour map of most active MMP-1 inhibitor. Positive potential areas in blue where more positively charged groups increase activity; Negative potential favored areas in red where more negatively charged groups increase activity. C. CoMSIA hydrophobic contour map of most active MMP-1 inhibitor the yellow contour for hydrophobic favor region, white indicates the hydrophilic favored region. D. CoMSIA acceptor contour map of most active MMP-1 inhibitor. The magenta contour for H-bond acceptor group increase activity, red indicates the disfavor region. E. CoMSIA donor contour map of most active MMP-1 inhibitor the cyan contour for H-bond donor favor region, purple indicates the disfavor region.

Table1: Structures, actual, predicted and residual activities from CoMFA and CoMSIA analyses

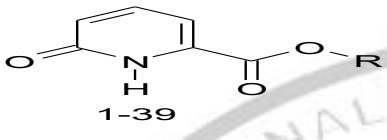

1-39

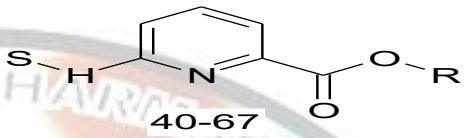

40-67

Mol. No.	R-group	IC 50	PIC 50	CoMFA		CoMSIA	
				Predicted	residual	Predicted	residual
1	Isopropyl	31	4.5	4.496	0.012	4.488	0.02
2	Cyclobutyl	25	4.6	4.491	0.111	4.488	0.114
3	$CH_2CHC(CH_3)_2$	37	4.43	4.323	0.108	4.455	-0.024
4	CH_2CCCH_3	50	4.3	4.49	-0.189	4.439	-0.138
5	Cyclohexyl	32	4.3	4.364	0.13	4.336	0.158
6*	Benzyl	30	4.52	4.344	0.176	4.371	0.149
7	$(CH_2)_2C_6H_5$	47	4.32	4.486	-0.159	4.612	-0.285
8*	4-Me-Benzyl	65	4.19	4.355	-0.165	4.103	0.087
9	3-CF_3-Benzyl	28	4.55	4.619	-0.067	4.645	-0.093
10	3-CF_3-Benzyl	24	4.55	4.538	0.081	4.601	0.018
11	3-OMe-Benzyl	69	4.62	4.436	-0.275	4.417	-0.256
12*	4-OMe-Benzyl	99	4	4.144	-0.144	4.079	-0.079
14*	$(CH_2)_4OC_6H_4$	67	4.17	4.084	0.086	4.056	0.114
15*	2-F-Benzyl	64	4.19	4.354	-0.164	4.319	-0.129
16	3-F-Benzyl	28	4.19	4.432	0.12	4.39	0.162
17	4-F-Benzyl	23	4.55	4.512	0.126	4.542	0.096
18	2,6-F-Benzyl	35	4.64	4.617	-0.162	4.636	-0.181
19*	2,5-F-Benzyl	70	4.15	4.249	-0.099	3.988	0.162
20	3,5-F-Benzyl	41	4.39	4.523	-0.136	4.385	0.002
21	2,4,6-F-Benzyl	16	4.79	4.541	0.254	4.585	0.21
22	2,4,5-F-Benzyl	30	4.52	4.61	-0.088	4.686	-0.164
23*	$CH_2C_6F_5$	19	4.72	4.61	0.11	4.615	0.105
24*	2-Cl-Benzyl	51	4.29	4.191	0.099	4.369	-0.079
25	3-Cl-Benzyl	25	4.6	4.612	-0.01	4.628	-0.026
26	4-Cl-Benzyl	26	4.58	4.643	-0.058	4.599	-0.014
27	2-Br-Benzyl	19	4.72	4.635	0.086	4.558	0.163
28	3-Br-Benzyl	22	4.66	4.53	0.127	4.632	0.025
29*	4-Br-Benzyl	81	4.09	4.008	0.082	4.187	-0.097
30*	Cinnamyl	86	4.07	4.101	-0.031	3.959	0.111
31*	1-Napthalyl	115	3.94	3.879	0.061	4.034	-0.094
32*	2-Napthalyl	75	4.12	4.013	0.107	4.024	0.096
33*	Piperonyl	128	3.89	3.962	-0.072	4.048	-0.158
34	3-Ph-Benzyl	42	4.38	4.321	0.055	4.286	0.09

35	3-OPh-Benzyl	68	4.17	4.308	-0.141	4.331	-0.164
36	2-Thiophenyl	56	4.25	4.414	0.107	4.296	0.225
37	3-Thiophenyl	39	4.4	4.413	-0.005	4.442	-0.034
38	2-Furyl	46	4.33	4.271	0.066	4.119	0.218
39	$(CH_2)_4CH_3$	50	4.3	4.395	-0.095	4.472	-0.172
40	Isopropyl	121	3.91	4.011	-0.094	3.931	-0.014
41	Cyclobutyl	135	3.87	3.914	-0.045	3.963	-0.094
42	Cyclohexyl	102	3.99	3.947	0.044	4.085	-0.094
43	Benzyl	101	3.99	4.08	-0.085	3.978	0.017
44	$(CH_2)_2C_6H_5$	120	3.92	4.032	-0.112	3.952	-0.032
45	$(CH_2)_3C_6H_5$	95	4.02	4.007	0.015	3.975	0.047
48	3-CF_3-Benzyl	134	3.87	3.842	0.03	3.947	-0.075
50*	3-OMe-Benzyl	86	4.07	3.985	0.085	3.995	0.075
51	4-OMe-Benzyl	108	3.96	3.854	0.112	3.801	0.165
52	$(CH_2)_4OC_6H_5$	138	3.86	3.876	-0.016	3.862	-0.002
53	3-F-Benzyl	119	3.92	3.894	0.03	3.93	-0.006
54	4-F-Benzyl	120	3.92	3.935	-0.015	3.925	-0.005
55	2,6-F-Benzyl	92	4.03	3.958	0.078	3.944	0.092
56	2,5-F-Benzyl	114	3.94	3.926	0.017	3.923	0.02
57	2,4,5-F-Benzyl	124	3.9	3.937	-0.031	3.933	-0.027
58	$CH_2C_6F_6$	78	4.1	4.087	0.02	3.828	0.279
59	4-Cl-Benzyl	126	3.89	3.878	0.021	3.998	-0.099
62	2-Napthalyl	99	4	4.071	-0.067	4.049	-0.045
63	4-Ph-Benzyl	119	3.92	3.963	-0.039	3.93	-0.006
64	3-Ph-Benzyl	75	4.12	4.09	0.034	3.983	0.141
65	3-OPh-Benzyl	78	4.1	4.057	0.05	4.044	0.063
66	4-OPh-Benzyl	114	3.94	4.02	-0.077	3.985	-0.042
67	3-Thiophenyl	108	3.96	3.982	-0.016	3.987	-0.021

*** Test set molecule**

Table 2: components used in the pls analysis, *SEE*-standard error estimation, *f value*- F-statistic for the analysis

Component	CoMFA		CoMSIA	
q^2	0.876		0.829	
r^2	0.968		0.983	
N	5		6	
F-Value	244.63		383.035	
*SE*E	0.055		0.041	
CV	0.872		0.793	
Bootstrap	*Mean*	*Stddev*	*Mean*	*Stddev*
SEE	0.046	0.003	0.035	0.021
r^2	0.977	0.011	0.986	0.005

q^2- LOO cross-validated correlation coefficient, r^2- non-cross-validated correlation coefficient, *n*- number of